Antimony-doped SnO_2-polythiophene photocatalyst: synthesis, characterization, and optimization for sunlight-driven dye degradation

M. Bibi [a], N. Nadeem [a], S. Noreen [a], Z. A. Rehan [b], B. F. Felemban [c], G. Mustafa [d], H. T. Ali [c], M. Zahid [a,*]

[a] *Department of Chemistry, University of Agriculture, Faisalabad- 38040 Pakistan*
[b] *Department of Chemistry, College of Science, Sultan Qaboos University Al-Khoud-123, Oman*
[c] *Department of Mechanical Engineering, College of Engineering, Taif University, Kingdom of Saudi Arabia*
[d] *Department of Chemistry, University of Okara, Pakistan*

Antimony-doped Tin Oxide (ATO) and its nanocomposite with polythiophene (PTh) were studied for Methylene blue (MB) degradation. The prepared photocatalysts were characterized using UV-Vis spectroscopy, FTIR, SEM-EDX, as well as XRD. The photocatalytic activity was examined under ambient sunlight and optimized conditions were found to be neutral pH, composite dose (30 mg/100mL), and H_2O_2 (5 mM) using ATO-PTh nanocomposite. MB was effectively degraded (~98%) within 90 min under optimized conditions. The degradation was studied through radical scavenging, reusability, and degradation kinetics. The response of different influencing parameters for degradation of dye by nanocomposites was assessed using the response surface methodology.

(Received August 28, 2024; Accepted February 7, 2025)

Keywords: Nanocomposite, Antimony-doped Tin Oxide (ATO), Photocatalysis, Conducting polymer, Visible light

1. Introduction

Water scarcity and organic pollution are major issues for both the global environment and developing nations. Even though the earth is covered in water to a depth of more than 70%, only 3% of this water is for human utilization, with the leftover 97% being salt water [1]. About 4 billion people all over the world face water shortages for at least one month annually [2]. The serious water shortage that has resulted from the fast-expanding industrialization of developing nations has turned into a problematic situation [3]. The main cause of water contamination is waste produced by a variety of businesses, including the metallurgical, mining, textile, and chemical industries [4, 5]. There are many different kinds and concentrations of water contaminants, including inorganic substances like ammonia, heavy metals, and phosphates as well as chemical fertilizers and organic substances like dyes, pesticides, pharmaceutical residues, and petrochemicals-hydrocarbons [6].

These wastes are carcinogenic and mutagenic compounds, and depending on how much is dumped, they may pose health risks. Due to their constancy in ambient settings, these dyes have the potential to produce a serious environmental problem. Additionally, the dye has the potential to irritate and induce allergic dermatitis. Certain pollutants have been found to cause cancer and mutations in both humans and aquatic organisms. More specifically, methylene blue has the potential to cause certain adverse effects in humans, including increased heartbeat, shock, and cyanosis [7]. For these reasons, finding an appropriate approach to get rid of the pollutants connected to coloring remains a difficult task.

Wastewater has been cleaned and disinfected using a variety of remediation techniques for many years [8-11]. The most efficient and environmentally beneficial of these technologies for treating and disinfecting wastewater are advanced oxidation processes (AOPs) [12, 13]. Because semiconductor metal oxides and sulfides have a variety of uses as photocatalysts, heterogeneous

* Corresponding author: rmzahid@uaf.edu.pk
https://doi.org/10.15251/JOR.2025.211.109

photocatalysis utilizing these materials to create sunlight-active catalysts has garnered interest over the decade [14]. The heterogeneous semiconductor metal oxides exhibit outstanding photocatalytic degradation when exposed to visible light [15-17]. Yet, their photocatalytic activity is limited to the visible portion of the spectrum due to their bandgaps. Because of its capacity to disseminate the active site upon the catalyst's surface, the production of active catalyst support is currently a hot topic. Since the support offers a broad surface for applying the primary photocatalytic test solutions, it may also improve the procedure [18].

Tin oxide (SnO_2) is a semiconductor oxide with an n-type structure and has a large energy of bandgap [19, 20]. Regardless of the high potential of tin oxide for photocatalytic applications, the pure material's practical usability is constrained by the compound's high activation energy (equivalent to ultraviolet light exposure) and the rapid recombination rate that occurs between photo-generated (e^-CB) as well as holes (h^+ VB). It is necessary to avoid electron/hole pair recombination to facilitate industrial applications and improve photocatalytic activity. The SnO_2 structure, including the band structure, is altered by the dopant antimony (Sb). After the Sb atom is added to the tin oxide solution, the lattice structure of SnO_2 significantly thickens. As the number of crystal lattice planes rises, so does the nanomaterial's electron conductivity [21]. Antimony, tin, and oxygen make up the ternary composition of the severely doped n-type semiconductor known as ATO. Because of their superior electrical conductivity and cheaper production cost in comparison to other doped forms of tin oxide including fluorine-doped and indium-doped tin oxide, the application of ATO nanoparticles in many fields of research and technology is quickly expanding [22].

Sb^{5+} (Pentavalent) can substitute Sn^{4+} (tetravalent) ions owing to their alike ionic radii (Sb^{5+} 0.065 nm and Sn^{4+} 0.071 nm) [23]. Usual n-type conductivity with an elevated charge carrier density and a wide optical gap was demonstrated by Sb-doped SnO_2. Antimony doping SnO_2 can also increase photocatalytic activity by reducing the rate at which holes/electrons couples recombine. Antimony serves as a hole/electron pair trap, causing the photocatalyst to separate charges more quickly. The wavelength that comprised both visible and UV spectrums, the antimony/tin oxide nanocomposite demonstrated decreased resistance and maintained its transparency. A study looked into the photocatalytic degradation of 0.6-weight percent antimony-doped tin oxide in the process of phenol degradation when exposed to sunlight [24].

Owing to their distinctive qualities like their easy synthesis methodology, adjustable morphology, excellent electrorheological property, porous structure, non-toxicity, unique redox chemistry, etc.—conjugated polymers, especially polythiophene or its derivatives/analogs, have been used extensively in wastewater treatment [25]. Because of its cost-effectiveness, easy processability, excellent thermal and environmental stabilities, ease of polymerization, and high electrical conductivities, the most attractive conductive polymers are polythiophene and its derivatives. [26-28].

This research aimed to synthesize novel ATO-PTh nanocomposites and apply them to the degradation of MB dye. The photocatalyst ATO was made by oxidation co-precipitation hydrothermal process and in situ polymerization in the presence of ATO nanoparticle to make ATO-PTh, and they were thoroughly examined utilizing various analytical methods, including FTIR, XRD, and SEM/EDS analysis. UV/vis spectrophotometry was used to measure the optical response of synthesized nanocomposites and to estimate the energy of bandgap. Using the pH drift method, the surface charge (pHpzc) of ATO-PTh nanoparticles was identified. The fabricated nanocomposite is used for wastewater treatment with effective utilization as a photocatalyst. Numerous parameters including, the solution's pH, initial dye concentration (IDC), catalyst dose and irradiation time. The sunlight was employed as the source of irradiation, although the impact of UV light was also investigated under optimized conditions. The statistical approach (response surface methodology) was used to estimate the individual as well as mutual impacts of various variables.

2. Materials and methods

2.1. Chemicals

Tin chloride pentahydrate ($SnCl_4.5H_2O$, Strem Chemicals, ≥98%), Hydrogen peroxide(H_2O_2, 30% w/w), Ammonia water (NH_3H_2O), Antimony chloride ($SbCl_3$, Riedel-de Haën,

≥99%), Anhydrous iron chloride ($FeCl_3.6H_2O$, reagent grade, ≥98%), HCl (35% w/w), NaCl (BioXtra, ≥99.5%) and sodium hydroxide (Sigma-Aldrich, ≥98%). Ethanol (98%) was purchased from Merck. Thiophene ($C_4H_4S_9$) was purchased from (UNI-CHEM) reagents. Methylene blue (MB), a model pollutant, was acquired from Fischer Scientific company.

2.2. Synthesis of ATO

The oxidation co-precipitation hydrothermal methodology was used to synthesize ATO nanoparticles. The key ingredients in the synthesis process were Antimony chloride ($SbCl_3$) and tin chloride ($SnCl_4$), which served as the source for Sb^{3+} and Sn^{4+} ions respectively. Weighed amounts of $SnCl_4.5H_2O$ and $SbCl_3$ were dissolved in 30 mL C_2H_5OH and 30 mL H_2O_2. The latter solution was poured into the first while being magnetically stirred. The $NH_3.H_2O$ was added to the above solution (dropwise) until white precipitates were formed. The white-colored ppts were then rinsed with ultrapure water until the silver nitrate test revealed no chlorine ions. The resulting white precipitates were then dissolved in water, shifted to a stainless-steel autoclave lined with 100 mL PPL, and undergo heating at 260 °C for 12 hr. The resulting blue PPT was repeatedly washed with ultrapure water, centrifuged, and dried. Lastly, the dry precipitate was ground into powders.

2.3. Preparation of PTh-ATO nanocomposite (NCs)

Thiophene monomer underwent in situ polymerization in the presence of ATO nanoparticles to make the ATO-PTh NCs. In a typical synthesis, chloroform was mixed with ATO NPs and thiophene. Under vigorous stirring, anhydrous $FeCl_3$ was added to chloroform. The reaction was magnetically stirred at room temperature for 24 hrs, during this time the color of the reaction mixture was changed from grey to black. To get rid of unreacted oxidants as well as monomers, the precipitates were washed with methanol and distilled water after being recovered by filtration and then dried in a heating oven under air [29]. A detailed schematic sketch of the synthesis procedure is presented in Figure 1.

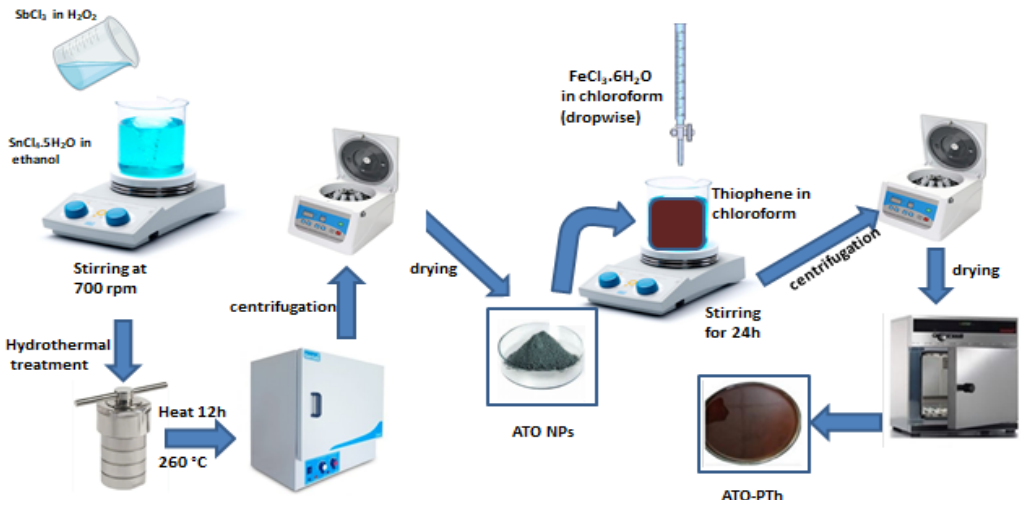

Fig. 1. Synthesis of ATO NPs and ATO-PTh NCs.

2.4. Characterization of photocatalysts

Various analytical methods were used to characterize the synthesized photocatalysts. All of the photocatalysts' crystal phase analyses were performed with X-ray diffractometer (Ultima-IV; Rigaku, Japan) operated at 40 kV and 40 mA with Cu-K radiation (= 0.154056 nm). The Deby-Scherrer equation was used to determine the grain size. FTIR spectroscopic analysis was carried out to see the catalysts' surface functionalities using a Spectrum 100, PerkinElmer FT-IR spectrometer. The optical response and the bandgap energies of the fabricated photocatalysts were determined using UV-visible spectroscopy. The absorption spectra for treated and untreated dye solutions were measured using a UV-Vis CECIL CE 7200 spectrophotometer.

The surface absorption of organic pollutants over the photocatalyst is greatly influenced by its surface charge. By applying the pH drift method, the pHpzc is determined. The point at which the photocatalyst's surface carries zero charge is called the pHpzc. The material's surface charge is negative at pH values greater than pHpzc, whereas it turns positive at pH values less than pHpzc. In this manner, the mechanism of anionic and cationic pollutant adsorption can be better understood. Antimony-doped tin oxide polythiophene composite displayed pHpzc at solution pH of 4 (Figure 5a). Since MB is a cationic dye, the negative charge on the surface of the catalyst encourages adsorption at a pH greater than the PHpzc.

2.5. Photocatalytic degradation experiments

The MB degradation was evaluated by ATO-PTh nanocomposites when exposed to sunlight. In the beginning, several feasibility tests were carried out to establish the activity of photocatalyst. The degradation experiments were carried out using a 50 ppm MB dye solution. The dye (MB) solution and the catalyst were placed in beakers and dispersed ultrasonically. The samples were kept in the dark for half an hour to establish the adsorption-desorption equilibrium stage between dye molecules and the catalyst surface. After 30 minutes, a small portion was executed, and centrifuged, and the adsorption capacity was assessed. The entire experimental setup was exposed to sunlight directly to start the photocatalytic degradation. The impact of numerous factors, containing pH (2–9), photocatalyst dose (10–60 mg/100 mL), dye concentration (10–90 ppm), oxidant dosage (1–20 mM), as well as time (0- 90 min), was investigated for degradation under sunlight. Following the completion of a specific experiment, the composites were separated using centrifugation using 10 mL from the reaction solution. The photocatalytic activity of the ATO and ATO-PTh photocatalysts was assessed in UV chambers. The degradation (%) was calculated from the following formula:

$$Degradation\ (\%) = 1 - \frac{C_t}{C_0} \times 100 \quad (1)$$

Here, C_t is the treated dye concentration and C_0 is the initial concentration of dye solution. The amount of sunlight was measured using light meter (HS1010A) and solar power meter (SM206).

2.6. Reaction kinetics for removal of MB

The reaction kinetic models (first and second-order) were employed to study the reaction kinetics. The expressions for these models are presented in Eq (2) and (3) for 1st and 2nd order kinetic studies.

$$ln\frac{C_o}{C_t} = kt \quad (2)$$

$$\frac{1}{C_t} - \frac{1}{C_o} - kt \quad (3)$$

2.7. Response surface methodology

RSM can be used to predict a response by analyzing two or more input variables. For this model, three variables (i.e., pH, H_2O_2 Conc., and photocatalysts Con.) were chosen. The interactions between all the independent variables at various levels were taken by considering the optimization of the parameters study. Design of Experiments (DoE) tools and RSM offer more precise results than the other approach of one factor-at-a-time (OFAT), it also minimizes the total experimental tries and generates better data values. In addition, DoE favors the connection between many factors to be considered and the variant test conditions for optimization thereby improving behavior.

3. Results and discussions

3.1. Characterization of ATO and ATO-PTh photocatalyst

XRD technique is used to analyze the phase of crystallinity of the composite. It also gives information about the dimensions of the unit cell. According to the X-ray diffractogram (XRD) characteristics, the intensity peaks were found near 26°, 28.08°, 31°, 33.98°, 49°, and 51.2°, which correspond to the (hkl) values of the peaks (100), (101), (200), (004), (110), and (201) [30]. The principal peaks present in ATO also present in ATO-PTh hybrids, however, the peaks weren't as strong as ATO, possibly due to a potential interaction between PTh and ATO (Figure 2b).

To identify the groups that are responsible for the stability and capping of NPs, the FT-IR spectrum of the synthesized ATO and ATO-PTh nanoparticles, measured in the 4000–400 cm^{-1} frequency range. The absorption peak near 800 cm-1 is attributed to the Sb-O. The peaks near 690 cm-1 may represent the O-Sn-O. The C-H stretching vibration caused the IR absorption peak near 1050 cm^{-1} to be visible in the fingerprint region of PTh, confirming the polymerization of the thiophene monomer. The existence of thiophene monomer is indicated by the absorption peak near 900 cm^{-1}, which is attributed to the C-S bending mode (Figure 2a).

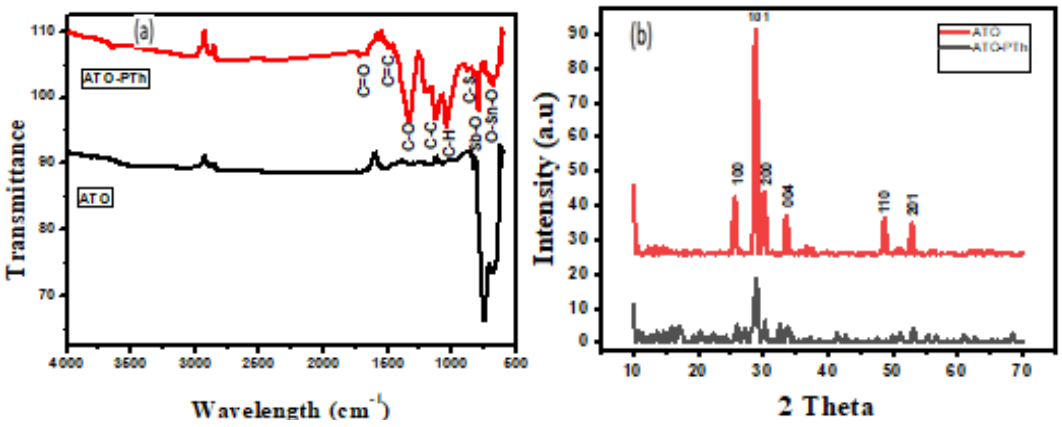

Fig. 2. (a) FTIR, and (b) XRD spectrum of ATO as well ATO-PTh.

The structural characteristics of the specimens were assessed through SEM imaging. The addition of ATO particles into the PTh matrix (Figure 3b) led to the development of an irregular morphology in the composite. Compared to pristine ATO NPs (Figure 3a), the composites exhibited heightened roughness and uneven surfaces, which are believed to contribute to their enhanced efficiency. This increased roughness and unevenness offer superior adsorption sites for contaminants when compared to even or smooth surfaces. The escalating surface roughness also leads to enhanced fractional dimensions, fostering enhanced surface interaction than planar surfaces. The elemental distribution of the ATO was elucidated through EDX analyses. The EDX of ATO (Figure 3c) presents a major contribution of Sb, Sn, and O in composition whereas, a little contribution of Na, and Cl ions could be due to impurities left due to precursor materials.

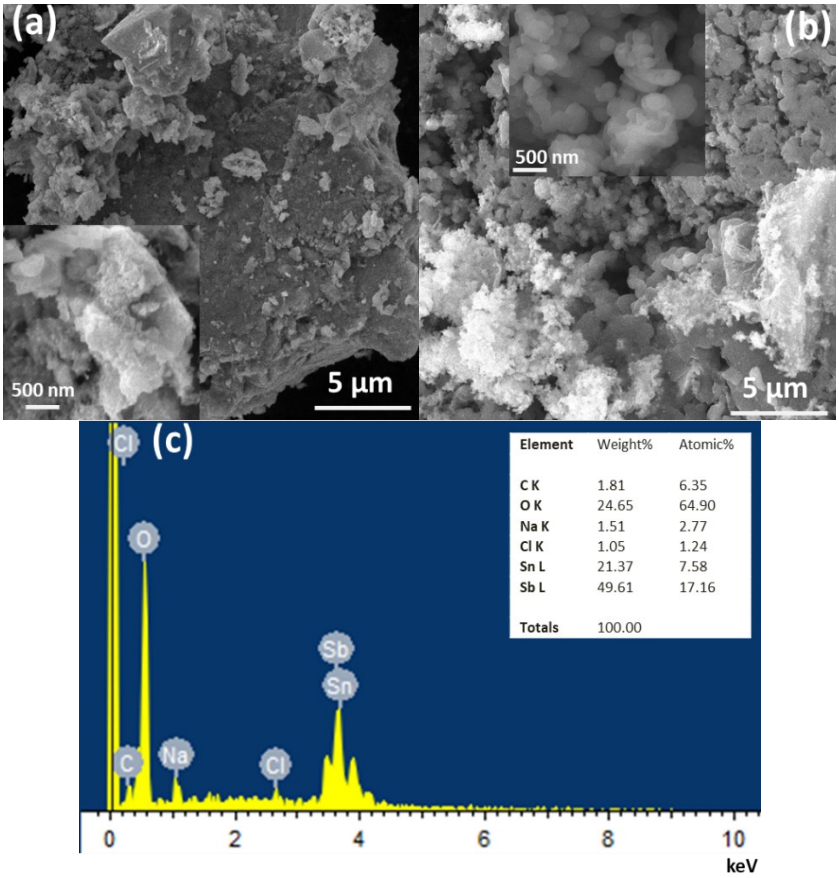

Fig. 3. SEM images of (a) ATO, (b) ATO-PTh, and (c) EDS of ATO NPs.

Determining the photocatalyst's optical characteristics is crucial for analyzing the catalytic activity under the considered light sources. Thus, bandgap measurements using UV-visible spectroscopy were done and the results are presented in Figure 4.

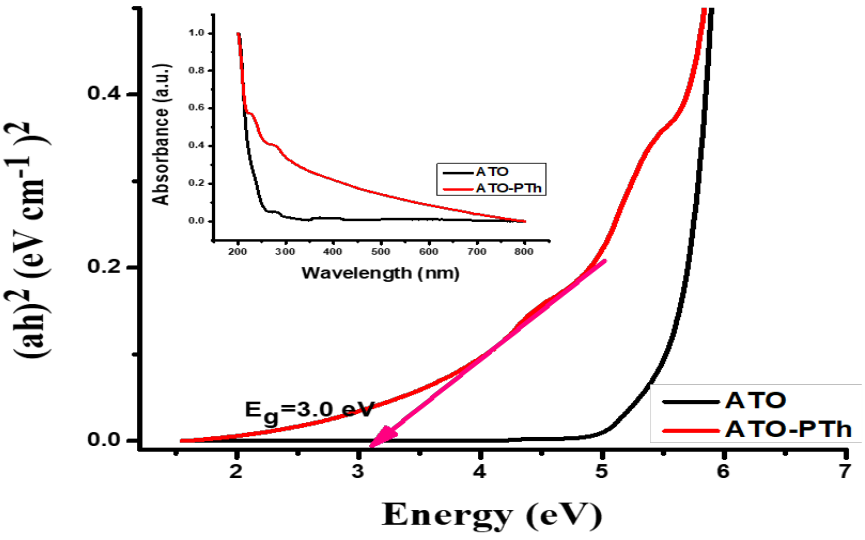

Fig. 4. Band gap of a) ATO b) ATO-PTh composite.

The inset of the figure contains UV-visible scans with the main plot of the band gap energy computed from the Tauc plot method. The band gap of ATO-PTh was found to be smaller (3.0 eV) compared to pristine ATO, and the wavelength shifted to higher wavelengths with lower energy. This not only shifts the photocatalyst's response towards visible light but also assists the generation of charge carriers at shorter wavelengths. The insertion of the PTh network in ATO also facilitates the prevention of charge recombination.

3.2. Effect of various working parameters on MB degradation

3.2.1. pH effect

The pH of a solution is the key element in the photocatalytic degradation process. The pH controls the surface charge characteristics of NCs based on the point of zero charge. The pH also affects the adsorptive ability of organic dye on the catalyst [31]. The molecules of methylene blue (cationic dyes), acquire a positive charge when they dissolve in water. ATO-PTh has a point of zero charge of 4. A lower value of pH than PHpzc results in electrostatic repulsion due to positively charged dye (MB) molecules and positively charged catalyst surface [32]. Furthermore, less hydroxyl is produced in acidic media. The dye (MB) molecules rapidly attracted to the photocatalyst's surface when pH > pHpzc. As a result, the capability of dye molecules to quickly adsorb on the catalytic surface is improved.

The effect of solution's pH on MB degradation is shown in Figure 5(b). The results represented that at neutral and basic pH, the degradation efficiency was greater than the acidic pH. This is because, in the solution having acidic pH, $H^{\cdot}$ ions react with cationic molecules of dye to compete for the adsorption onto the surface of the dye (adsorbent). As pH rises from 2-9, the cationic dye molecules interact more strongly with the negatively charged surface in the basic environment. Consequently, the adsorption of the cationic dye and its degradation is enhanced. The maximum degradation (98%) occurs at pH 7(neutral).

3.2.2. Catalyst dosage effect

To accurately predict the photocatalytic degradation rate for the efficient degradation of dye effluent, an optimal catalyst quantity is required. The higher degradation is caused by a higher amount of photocatalysts, which generate more active sites and, as a result, more active radicals. However, rising above the optimum dose shows a dramatic drop in photocatalytic degradation that slows down the reaction rate. Additionally, further increase could make the reaction mixture opaque, which would prevent light from penetrating and dispersing across a substrate's surface [33]. Minimizing excessive catalyst use is also essential in determining the viability of the entire process along with cost-effectiveness [34]. Overloading the metal will cover the active site upon that surface and reduce separation capacity; it may also serve as a recombination hub [35].

The effect of catalyst dose on MB degradation proficiency is represented in Figure 5(c). The photocatalyst ATO-PTh in the present study demonstrated the highest degradation at a dose of 30 mg/100 ml.

3.2.3. Oxidant dosage effect

The effect of oxidant dose on MB degradation is displayed in Figure 5(d). With both the photocatalyst and composite, catalyst degradation potential was speeded up until oxidant concentration reached a certain level (optimized value). The optimum amount of oxidant dose increases degradation as it produces the active species needed to degrade the contaminants.

The reaction for producing hydroxyl radicles by hydrogen peroxide is shown below in the equation, which also serves as an electron acceptor from the CB and aids in the separation of charges.

$$H_2O_2 + O_2^{-\cdot} \rightarrow O_2 + HO^{\cdot} + HO^{\cdot} \quad (4)$$

$$H_2O_2 + e^-(CB) \rightarrow HO^{\cdot} + HO^- \quad (5)$$

$$H_2O_2 + hv \rightarrow 2HO^{\cdot} \quad (6)$$

The energy that is absorbed is released via heat due to the increased e/h+ recombination if reactive species (such as oxygen or hydrogen peroxide) are not present or present in very small quantities near the photocatalyst's surface. Although, the presence of extra hydrogen peroxide facilitates the breakdown of H_2O_2 into oxygen and water. To achieve the highest photocatalytic effect, the optimal hydrogen peroxide dose is essential. With further increase in oxidant dosage above the optimum value results in the decline of dye degradation [36, 37]. This effect is caused by the production of less reactive hydrogen peroxide radicals ($HO_2^{\cdot}$) as compared to hydroxyl radicals which act as $HO^{\cdot}$ trappers.

$$HO^{\cdot} + H_2O_2 \rightarrow HO_2^{\cdot} + H_2O \quad (7)$$

$$HO^{\cdot} + HO_2^{\cdot} \rightarrow O_2 + H_2O \quad (8)$$

The excess H_2O_2 can create oxygen by interacting with valence band holes on the catalyst's surface, avoiding the formation of $HO^{\cdot}$ which lowers the overall degradation performance.

$$H_2O_2 + 2h^+ + VB \rightarrow O_2 + 2H^+ \quad (9)$$

3.2.4. Dye concentration effect

The impact of the concentration of dye on MB decomposition is illustrated in Figure 5(e). Several dye concentrations ranging from 10-90 ppm were studied on the degradation of MB. The inverse relationship between the dye concentration as well as degradation efficiency has been found. The maximum degradation was only possible at lower concentrations of MB [38]. Because more dye molecules are being adsorbed, as the dye load increases, the active sites on the catalyst surface become saturated. As a result, low light radiations enter the surface of the photocatalyst. So, fewer hydroxyl radicals are generated, which in turn results in a reduction in MB degradation. Furthermore, the transparency of the solution is influenced at higher dye concentrations. The oxidant-to-dye ratio decreases with increasing dye concentration, which has an adverse effect on photocatalysis.

3.2.5. Effect of radiation time in sunlight

The amount of time for dye deterioration was reduced by taking optimized condition of parameters containing oxidant dose, pH, catalyst dose and initial dye concentration. A UV-Vis spectrometer was used to measure the absorbance of the reaction solution every ten minutes while it was exposed to sunlight. It was observed that the degradation increases with time. Since with increase in irradiation time, the number of electrons, holes, and $O_2^{-\cdot}$ increase under the action of visible light [39]. The maximum degradation was observed after 90 minutes of the experiment under the sunlight as shown in Figure 5(f). Hence, 90 mins was chosen as the optimal time to show the maximum degradation efficacy of the methylene blue by using ATO-PTh as a catalyst.

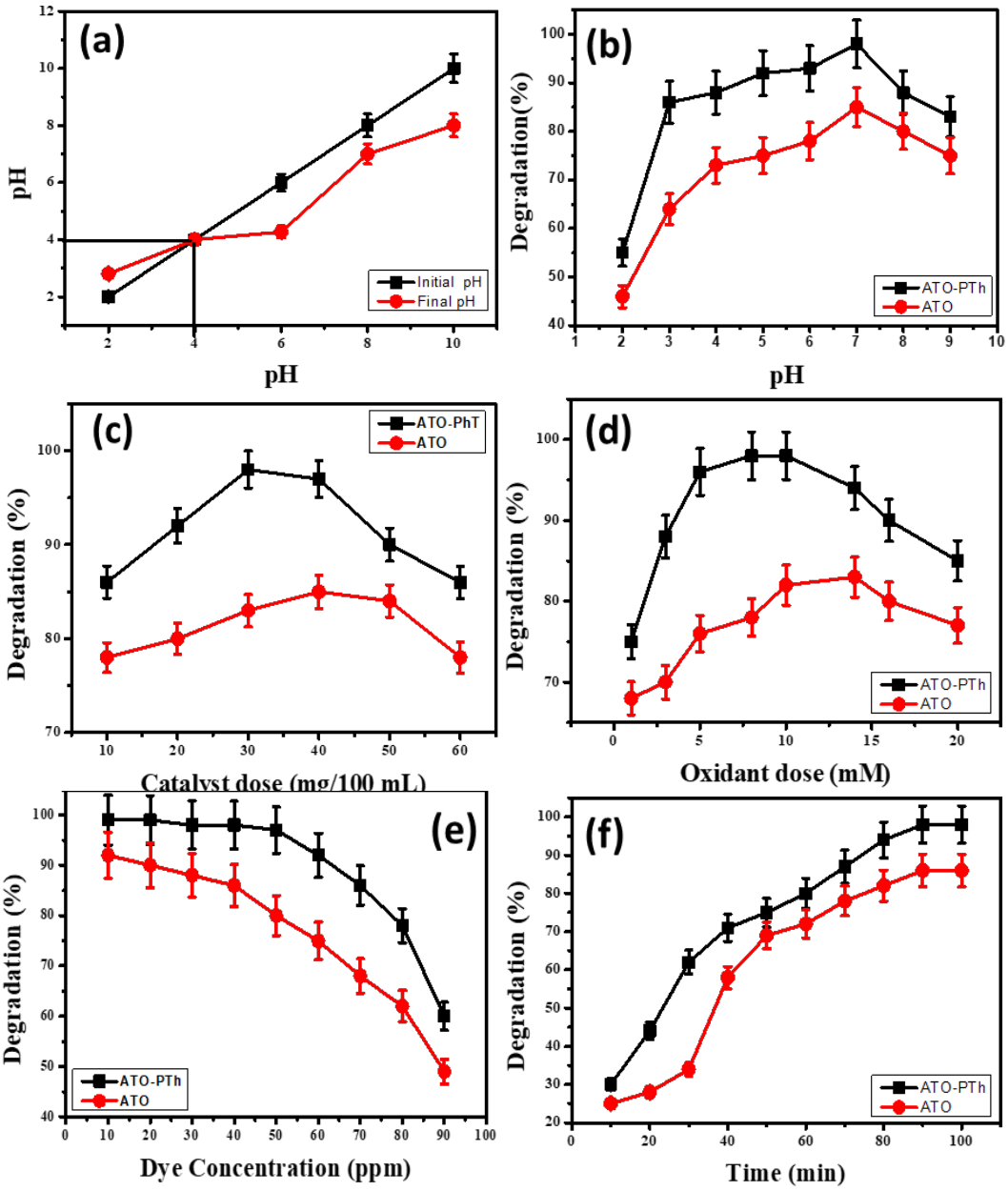

Fig. 5. Factors affecting the efficiency of degradation of photocatalysts (a) pH $_{pzc}$ (b) PH (c) catalysts dosage, (d) dye concentration, (e) oxidant dosage, (f) time.

3.2.6. Reusability, influence of irradiation source, and toxicity analysis of treated water

The heterogeneous catalyst showed outstanding efficacy even after being used manifold (Figure 6a). The remarkable proficiency of the nanocomposite might be because of its heterogeneous nature and stability when combined with the PTh matrix. In addition to pure ATO, the ATO-PTh composite exhibited enhanced stability. Five times the same catalyst was used, and following each cycle the composite was cleaned with ethanol and dried. The catalyst's improved stability allows it to withstand a variety of circumstances. The proficiency of degradation was reduced less than the 5th run, however, it was maintained with continued exposure to sunlight. The catalysts lost during filtration and subsequent rinse could be the cause of the activity drop [40].

The light sources utilized for MB degradation were ultraviolet light (254 nm) and sunlight and the results are illustrated in Figure 6b. Under the ultraviolet light, the degradation (98%) was observed to be completed in 70 minutes as compared to sunlight (90 minutes).

Following primary and secondary treatment, wastewater is utilized for a variety of things, such as irrigation of food crops, landscapes, and gardens. However, the organic contaminants in the wastewater are converted to carbon dioxide during the tertiary treatment stage, which uses sophisticated oxidation techniques. Water from this procedure can then be utilized to replenish surface groundwater. Due to socioeconomic and environmental factors, the use of sunlight-active nanocomposites in the treatment of wastewater to grow edible crops is advancing. Determining the efficacy of magnetic nanocomposite treatment for pollutant degradation in dye-loaded wastewater under solar radiation is crucial. This is dependent on the type of byproducts that are produced. To do this, we treated the most sensitive wheat seedlings with methylene blue-treated water using ATO and ATO-PTh. To do this, we applied ATO and ATO-PTh treated methylene blue water to the wheat crop's most vulnerable seeds. Filter paper and seeds with glass covers were soaked in the 10 ml treated MB dye solution. For a whole day, the Petri dishes were kept at room temperature. The wheat seeds exhibited significant germination in less than two days as seen in Figure 6c. Furthermore, the fact that the seeds treated with MB-treated wastewater did not turn black indicates that, under the right circumstances, treated water is safe to use for crop irrigation.

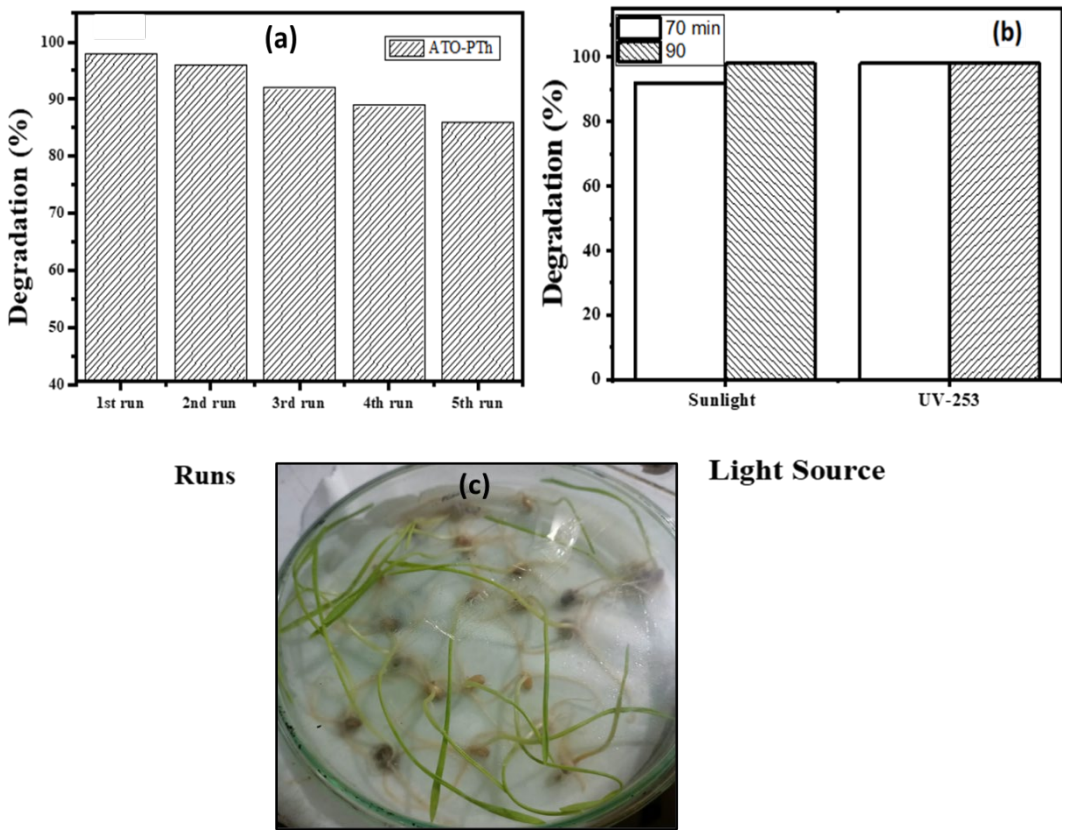

Fig. 6. (a) catalyst stability in terms of reusability, (b) effect of sunlight and UV irradiation of the photocatalytic performance of ATO-PTh NCs, and (c) Toxicity analysis and reuse of ATO-PTh treated water.

3.2.7. Effect of scavengers and proposed mechanism

The MB dye degradation is activated with certain reactive groups like electrons, OH radicals, holes, etc. The radical trapping experiment was carried out to identify the possible radicals involved in the dye degradation [41]. The 5ml of 10mM scavengers solutions comprising $K_2Cr_2O_7$ for electrons, EDTA for holes, ascorbic acid for O_2, and dimethyl sulfoxide (DMSO) for 'OH trapping was used.

Sunlight was used as a source of light to perform the experiment with optimized parameters. The results are illustrated in Figure 7a. The results clearly show that $K_2Cr_2O_7$ is the main scavenger in the process of degradation as it decreases the degradation efficacy from 98% to 50% using ATO-PTh as a photocatalyst. Furthermore, the superoxide radicals as well as hydroxide radicals were also seen to be active in degradation as the values lowered to 69% and 70% from 98% by the addition of Ascorbic acid and DMSO respectively. The little contribution of holes was seen and degradation efficiency was lowered from 98% to 85%. Taking into account the impact of holes, electrons, and radicals (superoxide and hydroxyl), the degradation scheme can be suggested as: In the photocatalytic process, sunlight with an Eev larger than the composite's energy bandgap creates the e-/h+ pairs. These holes result in the creation of 'OH radicals which are effective at breaking down dye molecules into fragments and then mineralizing them.

ATO-PTh increases photocatalytic activity by reducing the rate at which holes/electrons couples recombine. ATO serves as a hole/electron pair trap, causing the photocatalyst to separate charges more quickly. At a wavelength that comprises both the visible and UV spectrums, the h^+ is left within the VB as a result of the dye being initially adsorbed on the catalyst's surface (e.g. ATO-PTh) and then being subjected to visible light to stimulate valence electrons and enable their transfer from the valance band to the conduction band. On the photocatalyst's exterior, water molecules that are adsorbed react with holes (h^+) and electrons (e^-) to generate hydroxyl radicals, whereas, e^- transforms dissolved O_2 into superoxide anion radicals. The molecules of dye are broken down into less complex molecules like CO_2 and H_2O by these light-generated radicals. The reaction mechanism of the above discussion can be concluded as below:

$$ATO - PTh + hv \rightarrow e^- + h^+ \quad (11)$$

$$O_2 + e^- \rightarrow O_2^{-\cdot} \quad (12)$$

$$O_2^{-\cdot} + H^+ \rightarrow HOO^{\cdot} \quad (13)$$

$$2HOO^{\cdot} \rightarrow H_2O_2 + O_2 \quad (14)$$

$$O_2^{-\cdot} + H_2O_2 \rightarrow O_2 + HO^{\cdot} + HO^- \quad (15)$$

$$H_2O_2 + hv \rightarrow 2HO^{\cdot} \quad (16)$$

$$HO^{\cdot} + h^+ \rightarrow H^+ + HO^{\cdot} \quad (17)$$

$$H_2O + h^+ \rightarrow H^+ + HO^{\cdot} \quad (18)$$

$$Pollutants + \{HO^{\cdot}, e^-, h^+, HOO^{\cdot}, O_2^{-\cdot}\} \rightarrow Degraded\ products \quad (19)$$

The photocatalytic breakdown of MB dye under exposure to visible light was used as a light source to evaluate the photocatalytic capability of the photocatalyst. The mechanism of degradation of Methylene blue is shown in Figure 7b.

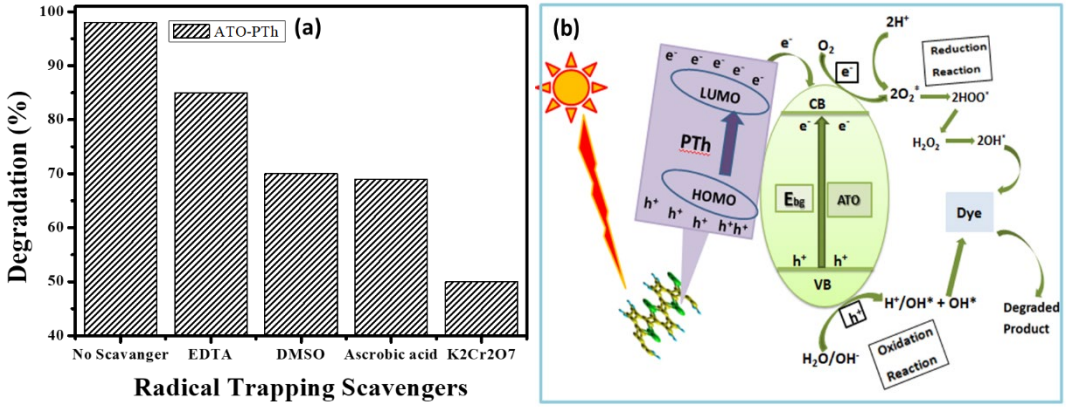

Fig. 7. Effect of radicle traping scavengers on photocatalytic efficiency and (b) proposed photocatalytic degradation mechanism from ATO-PTh NCs.

The Plots in Figure 8 related ln (C_o/C_t) with time (irradiation) when different amounts of catalysts are used for MB degradation show a straight line. In this case, the starting concentration is denoted by (C_o) and the final concentration by (C_t) in first-order kinetics, as seen in Figure 8a. Effective first-order reaction kinetics are followed in the MB photo-degradation process by both ATO as well as ATO-PTh. When (C_o/C_t) is plotted against time, a straight line shows that the model fits the data well, and the slope of line is equal to the first-order rate constant (k). The greater k of all T shows that both composites' MB degradation was effective in the presence of sunlight. The R^2 values of ATO (0.99) and ATO-PTh (0.98) show that both composites follow the first-order kinetic model.

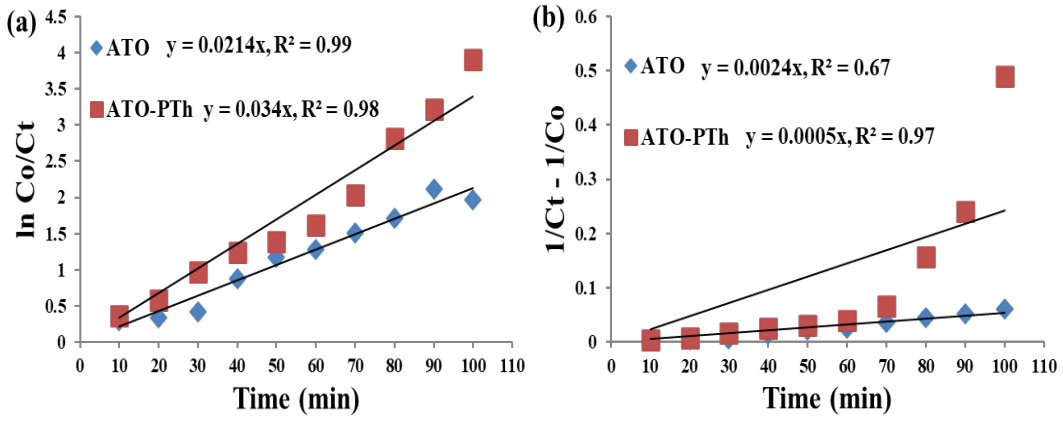

Fig. 8. Kinetic study (a) 1st order and (b) 2nd order Kinetic models for ATO and ATO-PTh.

3.3. Parameter interaction and optimization via RSM

The primary goal of the RSM is to optimize parameters and investigate the influence of several interacting factors on the degradation of Methylene blue (MB). The parameters including pH (2–9), catalyst dose (10–60 mg/100 mL), as well as IDC (10–90 ppm), were taken into account for catalyst optimization under sunlight using central composite design (CCD). ANOVA was applied to observe the significance of the model and the impact of the parameters. A certain range for these values was used to create the contour and 3D diagrams.

The fit summary plot demonstrates the high degree of significance of the developed model. The R2 value can be used to calculate the model's significance which is approximately equal to one. This quadratic model was used to calculate the percent degradation and the efficiency of the selected

variables. The contour diagrams and three-dimensional response surface, as seen in Figure 9, are used to illustrate the way two parameters interact to affect MB degradation. This process involved changing two factors while keeping the third constant, keeping the parameters within ranges. By modifying the upper and lower limits, the largest response for degradation was achieved. The 3-D surface plots of the removal of MB as a function of pH and catalyst dose, with the IDC held constant, are displayed in Figure 9(b). The pH of the solution as well as catalyst dosage showed the highest degradation at neutral pH and photocatalyst dose of 30 mg/100mL. Because more catalyst particles were occupying the active sites, there was a decrease in MB degradation as catalyst concentration rose. An interaction between catalyst dosage and pH had a significant impact on MB removal efficiency. Due to enhanced hydroxyl radical generation at higher pH values, the MB degradation efficiency was enhanced with a rise in dye starting concentration. A decrease in degradation efficiency was noted in Figure 9(a) due to a decrease in OH radicals resulting from a large number of pollutant molecules at pH greater than 8 and high dye concentration [42]. The pace of degradation is slowed down at greater concentrations of dye in a strongly alkaline media. The likelihood of producing mineral anion is also raised, which heightens the competition between different organic components to interact with OH radicals and slows down the degradation process as a whole [43], [44]. By maintaining the pH constant, Figure 9(c) illustrates the impact of catalyst dose and IDC on degradation percentage. Up to a specified number, at which it demonstrated the highest efficacy at a certain dye concentration, the degradation efficiency first rose as the concentration increased [12, 33]. Once the quantity of H_2O_2 is raised from 1 mM to 5 mM, the dye degradation increases steadily and then begins to slow down. The photocatalyst's surface is inhibited from the e^-/h^+ pair recombination due to the oxidant's positive effect while Hydrogen peroxide functions as a scavenger for hydroxyl radicals and holes in the VB at higher oxidant dosage concentrations.

3.3.1. Analysis of variance (ANOVA)

The model's significance is indicated by an F-value of 60.14 demonstrating only 0.01% probability that the F-value could be high due to noise. The ($p<0.0500$) designated the significance of model terms. The significant modal terms are A, B, C, AB, B^2, and C^2. The values (>0.1000) show the non-significance of model terms. The F-value of 2.12 suggests a non-significant Lack of Fit as compared to the pure error. The R^2 (predicted) of 0.8974 is in substantial agreement with the R^2 (adjusted) of 0.9655 (Table 1). The signal-to-noise ratio is measured with adequate precision. A ratio of more than 4 is preferred. An adequate signal is shown by a signal ratio of 21.977. Navigating the design space is possible with this size.

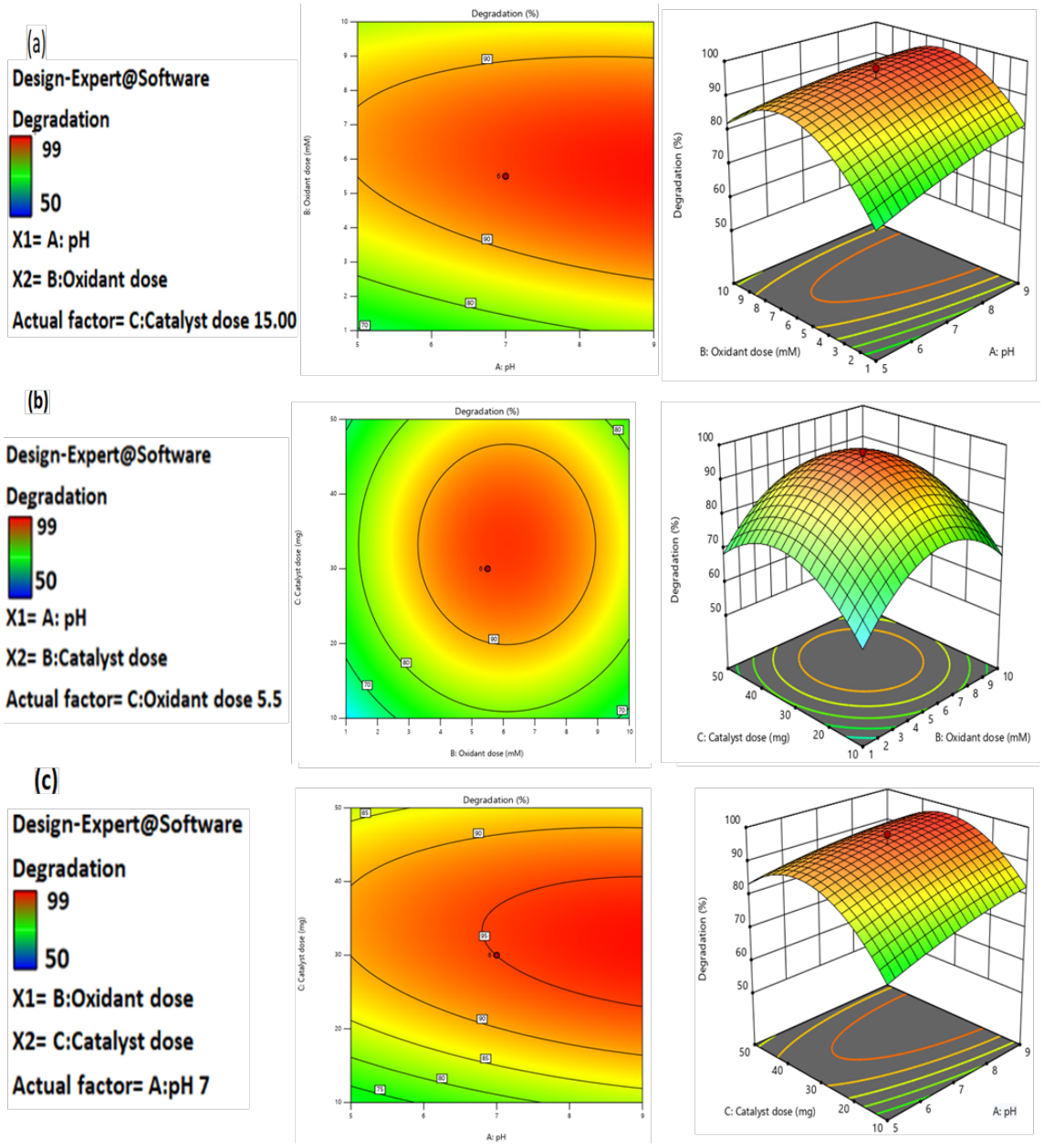

Fig. 9. Response surfaces (right side 3D surfaces, left side contour plots) representing the mutual effect of (a) pH and oxidant dose, (b) pH and catalyst dose (c) oxidant and catalyst dose.

The final equation in terms of coded factor is given as:

$$MB\ Degradation(\%) = +95.02 + 3.64 \times A + 3.87 \times B + 4.07 \times C - 2.50 \times AB - 1.75 \times AC + 0.0000 \times BC - 1.34 \times A^2 - 14.25 \times B^2 - 12.48 \times C^2$$

Table 1. ANOVA table for ATO-PTh.

Source	Sum of Square	Df	Mean Square	F-value	p-value	
Model	5410.59	9	601.18	60.14	<0.0001	Significant
A-pH	181.40	1	181.40	18.15	0.0017	
B-Oxidant dose	204.27	1	204.27	20.43	0.0011	
C-Catalyst dose	226.65	1	226.65	22.67	0.0008	
AB	50.00	1	50.00	5.00	0.0493	
AC	24.50	1	24.50	2.54	0.1485	
BC	0.0000	1	0.0000	0.0000	1.0000	
A^2	25.96	1	25.96	2.60	0.1382	
B^2	2925.09	1	2925.09	292.61	<0.0001	
C^2	2244.22	1	2244.22	224.50	<0.0001	
Residual	99.96	10	10.00			
Lack of fit	67.96	5	13.59	2.12	0.2140	Not Significant
Pure Error	32.00	5	6.40			
Cor total	5510.55	19				
Std Dev.	3.16		R-Square		0.9819	
Mean	75.85		Adj R-Square		0.9655	
CV%	4.17		Pred R-Square		0.8974	
PRESS			Adeq Precision		21.9772	

4. Conclusion

The ATO-PTh photocatalyst was synthesized via in-situ chemical oxidative polymerization with ATO nanoparticles. Various analyses, including UV/visible spectroscopy, FTIR, XRD, and SEM/EDS, were conducted. The surface charge of ATO-PTh NPs was determined using the pH drift method. Sunlight and UV light were used for irradiation under optimized conditions. Photocatalytic performance for degrading MB dye was assessed, considering factors like pH, oxidant and catalyst dose, IDC, and irradiation time. Under optimal conditions (pH 7, 5 mM oxidant, 30mg catalyst, 50ppm IDC), ATO-PTh achieved 98% degradation in 90 minutes, surpassing ATO (85%). The doped PTh reduced the band gap to 3.0 eV, enhancing visible light response. First and second-order reaction kinetics models were explored, and Response Surface Methodology (RSM) analyzed variable effects. The composite exhibited enduring efficiency in pollutant degradation, contributing to wastewater detoxification. Its enhanced optical properties open avenues for diverse applications, suggesting potential environmental reclamation. The study's simple synthesis method and effective photocatalysis make it adaptable for modifying different systems.

Author statement

Maryam Bibi: Data curation. Methodology, Writing- Original draft. Nimra Nadeem: Conceptualization, Visualization, Writing—review and editing. Saima Noreen: Investigation, Validation. Zulfiqar Ahmed Rehan: Software, Formal analysis. Bassem F. Felemban: Investigation. And Resources. Ghulam Mustafa: Methodology, Data curation. Hafiz Tauqeer Ali : Formal analysis, Validation. Muhammad Zahid: Supervision, Project administration, Writing—review and editing.

Competing interest

The authors declare that they have no competing interests.

Acknowledgments

The authors extend their appreciation to Taif University, Saudi Arabia, for supporting this work through project number (TU-DSPP-2024-321).

Funding

This research was funded by Taif University, Taif, Saudi Arabia, Project No. (TU-DSPP-2024-321).

References

[1] Ahmad, M., et al., Environmental science & technology, 2019. 53(4): p. 2161-2170; https://doi.org/10.1021/acs.est.8b05866

[2] Dongare, P.D., et al., Proceedings of the National Academy of Sciences, 2017. 114(27): p. 6936-6941; https://doi.org/10.1073/pnas.1701835114

[3] Shafiq, I., et al., Journal of Environmental Chemical Engineering, 2019. 7(4): p. 103265; https://doi.org/10.1016/j.jece.2019.103265

[4] Crini, G., E. Lichtfouse, Environmental Chemistry Letters, 2019. 17: p. 145-155; https://doi.org/10.1007/s10311-018-0785-9

[5] Burakov, A.E., et al., Ecotoxicology and environmental safety, 2018. 148: p. 702-712; https://doi.org/10.1016/j.ecoenv.2017.11.034

[6] Rashid, R., et al., Environmental Science and Pollution Research, 2021. 28: p. 9050-9066; https://doi.org/10.1007/s11356-021-12395-x

[7] Mishra, A.K., N.R. Agrawal, I. Das, Journal of environmental chemical engineering, 2017. 5(5): p. 4923-4936; https://doi.org/10.1016/j.jece.2017.09.017

[8] Liu, W., et al., Angewandte Chemie International Edition, 2008. 47(30): p. 5619-5622; https://doi.org/10.1002/anie.200800172

[9] Xu, X., et al., Applied Catalysis B: Environment and Energy, 2024. 345: p. 123701; https://doi.org/10.1016/j.apcatb.2024.123701

[10] Wang, N., et al., Separation and Purification Technology, 2025. 355: p. 129566; https://doi.org/10.1016/j.seppur.2024.129566

[11] Zhao, Y., et al., Green Chemistry, 2024. 26(5): p. 2645-2652; https://doi.org/10.1039/D3GC04566H

[12] Rahman, M.U., et al., Optical Materials, 2021. 120: p. 111408; https://doi.org/10.1016/j.optmat.2021.111408

[13] Dong, S., et al., Chemical Engineering Journal, 2022. 431: p. 133824; https://doi.org/10.1016/j.cej.2021.133824

[14] Abebe, B., et al., Inorganic Chemistry Communications, 2021. 123: p. 108343; https://doi.org/10.1016/j.inoche.2020.108343

[15] Harish, S., et al., RSC advances, 2017. 7(55): p. 34366-34375; https://doi.org/10.1039/C7RA04250G

[16] Shafi, P.M., et al., ACS Sustainable Chemistry & Engineering, 2017. 5(6): p. 4757-4770; https://doi.org/10.1021/acssuschemeng.7b00143

[17] Arfa, U., et al., Polymers, 2023. 15(13): p. 2775; https://doi.org/10.3390/polym15132775

[18] Shan, Z., et al., Frontiers in Chemistry, 2021. 9: p. 755836; https://doi.org/10.3389/fchem.2021.755836

[19] Ulyankina, A.A., A.B. Kuriganova, N.V. Smirnova, Mendeleev Communications, 2019. 29(2): p. 215-217; https://doi.org/10.1016/j.mencom.2019.03.034

[20] Sivakumar, S., E. Manikandan, B. Mahalakshmi, Vacuum, 2020. 173: p. 109116; https://doi.org/10.1016/j.vacuum.2019.109116

[21] Lee, H., S. Jin, and S. Yim, Journal of Physics and Chemistry of Solids, 2020. 138: p. 109264; https://doi.org/10.1016/j.jpcs.2019.109264
[22] Khorshidi, B., et al., Polymer, 2019. 163: p. 48-56; https://doi.org/10.1016/j.polymer.2018.12.058
[23] Al-Hamdi, A.M., M. Sillanpää, J. Dutta, Research on Chemical Intermediates, 2016. 42: p. 3055-3069; https://doi.org/10.1007/s11164-015-2197-9
[24] Al-Hamdi, A.M., et al., Applied Surface Science, 2016. 370: p. 229-236; https://doi.org/10.1016/j.apsusc.2016.02.123
[25] Huang, Y., et al., Rsc Advances, 2014. 4(107): p. 62160-62178; https://doi.org/10.1039/C4RA11496E
[26] Shokuhi Rad, A., Journal of molecular modeling, 2015. 21: p. 1-6; https://doi.org/10.1007/s00894-015-2832-9
[27] Ustamehmetoğlu, B., Electrochimica Acta, 2014. 122: p. 130-140; https://doi.org/10.1016/j.electacta.2013.12.130
[28] Jose, M.A., S. Varghese, M.J. Antony, In situ chemical oxidative polymerisation for ordered conducting polythiophene nanostructures in presence of dioctyl sodium sulfosuccinate. 2016.
[29] Murugavel, S., M. Malathi, Materials Research Bulletin, 2016. 81: p. 93-100; https://doi.org/10.1016/j.materresbull.2016.05.004
[30] Amutha, E., et al., Nanoscale Advances, 2023. 5(1): p. 255-267; https://doi.org/10.1039/D2NA00666A
[31] Alosaimi, E.H., et al., Journal of Chemistry, 2021. 2021: p. 1-18; https://doi.org/10.1155/2021/4660423
[32] Tahir, N., et al., Environmental Science and Pollution Research, 2022. 29(5): p. 6552-6567; https://doi.org/10.1007/s11356-021-16094-5
[33] Rubab, M., et al., Nanotechnology, 2021. 32(34): p. 345705; https://doi.org/10.1088/1361-6528/ac037f
[34] Yousefi, S.R., O. Amiri, M. Salavati-Niasari, Ultrasonics sonochemistry, 2019. 58: p. 104619; https://doi.org/10.1016/j.ultsonch.2019.104619
[35] Sinar Mashuri, S.I., et al., Catalysts, 2020. 10(11): p. 1260; https://doi.org/10.3390/catal10111260
[36] Enesca, A., et al., Applied Catalysis B: Environmental, 2014. 147: p. 175-184; https://doi.org/10.1016/j.apcatb.2013.08.016
[37] Visa, M., C. Bogatu, A. Duta, Journal of Hazardous Materials, 2015. 289: p. 244-256; https://doi.org/10.1016/j.jhazmat.2015.01.053
[38] Nadeem, N., et al., Applied Surface Science, 2021. 565: p. 150542; https://doi.org/10.1016/j.apsusc.2021.150542
[39] Li, J., et al., Nanotechnology, 2020. 31(12): p. 125101; https://doi.org/10.1088/1361-6528/ab5ba7
[40] Shen, R., et al., Chinese Journal of Catalysis, 2022. 43(10): p. 2453-2483; https://doi.org/10.1016/S1872-2067(22)64104-4
[41] Shao, P., et al., Environmental Science & Technology, 2020. 54(13): p. 8464-8472; https://doi.org/10.1021/acs.est.0c02645
[42] Tahir, N., et al., Journal of Environmental Management, 2023. 337: p. 117706; https://doi.org/10.1016/j.jenvman.2023.117706
[43] Thangavel, S., et al., Journal of Physics and Chemistry of Solids, 2017. 110: p. 266-273; https://doi.org/10.1016/j.jpcs.2017.06.005
[44] Fatima, A., Chalcogenide Letters, 2024. 21(11): p. 895-915. https://doi.org/10.15251/CL.2024.2111.895